

# Variability of depolarization of aerosol particles in Beijing mega city: implication in interaction between anthropogenic pollutants and mineral dust particles

5 Yu Tian<sup>1, 2</sup>, Xiaole Pan<sup>1,\*</sup>, Tomoaki Nishizawa<sup>3</sup>, Hiroshi Kobayashi<sup>4</sup>, Itsushi Uno<sup>5</sup>, Xiquan Wang<sup>1</sup>,  
Atsushi Shimizu<sup>3</sup> and Zifa Wang<sup>1,2,6</sup>

<sup>1</sup>State Key Laboratory of Atmospheric Boundary Layer Physics and Atmospheric Chemistry, Institute of Atmospheric Physics, Chinese Academy of Sciences, Beijing, 100029, China

<sup>2</sup>University of Chinese Academy of Sciences, Beijing, 100049, China

<sup>3</sup>National Institute for Environmental Studies, Tsukuba, Ibaraki, 305–8506, Japan.

10 <sup>4</sup>University of Yamanashi, Yamanashi, 400–0016, Japan.

<sup>5</sup>Research Institute for Applied Mechanics, Kyushu University, Kasuga, Fukuoka, 816–8580, Japan.

<sup>6</sup>Center for Excellence in Regional Atmospheric Environment, Chinese Academy of Science, Xiamen, 361021, China

*Correspondence to:* Xiaole PAN (panxiaole@mail.iap.ac.cn)

**Abstract.** East Asia is suffering from both severe air pollution problem due to intensive anthropogenic emissions and natural mineral dust aerosols. During transport, the aerosol particles undergo complex mixing processes, resulting in great impacts on regional air quality, human health and climate. In this study, we conducted a long-term observation using an Optical Particle Counter equipped with a Polarization detection module (POPC) at an urban site in Beijing. Mass concentrations of both PM<sub>2.5</sub> and PM<sub>10</sub> estimated from POPC compared well with ground-based measurements. The results revealed that the observed depolarization ratio ( $\delta$ , termed as the ratio of the intensity of the s-polarized signal to the intensity of the 120 degree backward scattering signal [ $s/(s+p)$ ]) for aerosol particles in the fine mode was generally much lower in summer than that in spring as a result of predominance of different aerosol types. Mineral dust particles in the coarse mode normally had a large  $\delta$  value ( $0.3 \pm 0.05$ ) owing to their non-spherical shape; however, particles in the fine mode consisted of large proportion water-soluble compositions, which lead to apparent decrease of their  $\delta$  values in particular high relative humidity (RH) condition. Because the observation site was subject to frequent impact of dust event in spring,  $\delta$  value of particle at 1  $\mu\text{m}$  was almost twice as high as that ( $0.07 \pm 0.01$ ) in summer. Based on size-resolved  $\delta$  values, anthropogenic pollutants, mineral dust and polluted mineral dust particles, and their contribution to local air quality were well distinguished. About 26.7% of substandard days (daily averaged PM<sub>2.5</sub> concentration larger than 75  $\mu\text{g}/\text{m}^3$ ) in Beijing was featured by high atmospheric loading of coarse-mode particles in winter-spring time. In particular during severe pollution episode in winter, the  $\delta$  values of coarse mode particles decreased by 13%, implies the high possibility of dust-related heterogeneous processes on pollution formation. During dust event,  $\delta$  values of particle at  $D_p = 5 \mu\text{m}$  decreased evidently with increase of PM<sub>2.5</sub>/PM<sub>10</sub> ratio as well as RH, indicating of the morphological changes of mineral dust. This study confirmed that high RH tends to promote water absorption processes on the dust surface as well as coating of soluble compounds, and suggested that complex mixing of dust and anthropogenic

particles may lead to underestimate impact of dust particles in urban area based on remote sensing technique, and interaction between dust particle and pollutants should be well considered by the optical model.

## 1 Introduction

5 Rapid economic growth and urbanization processes in East Asia has caused serious air pollution in the past decades owing to the substantial consumption of fossil fuel. Anthropogenic emissions (industrial, traffic, residential etc.) emits substantial amount of pollutant gases ( $\text{SO}_2$ ,  $\text{NO}_2$ ,  $\text{NH}_3$ , VOCs etc.) and primary aerosols (Akimoto, 2003;Akimoto et al., 2006;Kurokawa et al., 2013;Li et al., 2017), resulting in formation of  $\text{PM}_{2.5}$ . Mineral dust particles in the atmosphere also have a detrimental impact on air quality and human health such as reducing visibility, increase respiratory morbidity. Beijing is located in vicinity 10 of dust source region. In dry seasons, mineral dust particles emitted from Taklimakan, Gobi, Mongolia plateau and Loess Plateau may transport eastwardly across the northern part of China (Takemura et al., 2002;Jickells et al., 2005;Uno et al., 2009), and undergo complex mixing with anthropogenic pollutants.

The environmental and climate effects of these mixing processes are notable because of dramatic changes in the physical, chemical and optical properties of mixed particles (Pan et al., 2009). In polluted urban area, soluble salts coated on dust aerosols 15 reduce the critical supersaturation, and there is a stronger tendency for polluted aerosols to serve as CCN (cloud condensation nuclei), influencing the formation of cloud (Sullivan et al., 2009;Tang et al., 2016). The soluble salts are derived from directly trapping inorganic salt, as well as the heterogeneous reactions between reactive gases (mostly  $\text{HNO}_3$ ,  $\text{HCl}$ ,  $\text{SO}_2$  and  $\text{NO}_2$ ) and alkaline mineral dust. Continuous coating and hygroscopic growth processes on the surface modify the shapes of dust particles (Li et al., 2011). A recent study pointed out that coexistence of  $\text{NO}_x$  and mineral dust may lead to a gas-particle conversion 20 process and promote the conversion of  $\text{SO}_2$  to sulfate (He et al., 2014). There is also observational evidence that heavy dust mixed with anthropogenic pollution may trigger new particle formation(Dupart et al., 2012;Nie et al., 2014), which exaggerates the degradation of regional air quality. The above scientific discoveries all indicate the importance of study on the mixing states of dust and pollution aerosols.

Widely used technologies to distinguish aerosol types include high-precision ground-based Lidar (Light Detection And 25 Ranging) systems and satellite-borne observations (Cloud-Aerosol Lidar and Infrared Pathfinder Satellite Observation; CALIPSO)(Winker et al., 2009;Cesana et al., 2016;Venkata and Reagan, 2016) that measures an targeted air parcel's volume depolarization ratio from backward scattering signals. Aerosol types can be distinguished by the distinct parts formed by data points on a figure of their volume depolarization ratio( $\delta_a = s/p$ , at 532 nm) of aerosols versus backscattering color ratio (1064 nm/532 nm); however, bias in the classification of internal mixed dust (normally has a large color ratio and small  $\delta_a$ ) is 30 sometimes unavoidable since external mixing of a substantial amount of fine particles ( $\delta_a < 0.1$ ) with mineral dust aerosols ( $\delta_a > 0.35$ ) can also results in decrease of of  $\delta_a$  value. To respond to this need, an optical particle counter with a depolarization module was developed. Single particle  $\delta$  value measure is able to quantitatively investigate the evolution of the mixing of

dust particles during their transport (Pan et al., 2015). According to the size-resolved  $\delta$  value of scattering signals, particles in spherical shape can be distinguished because the direction of polarization of scattering light was identical with the incident light; for the non-spherical particles, direction of polarization will be deviated significantly. Generally, secondary formatted particles tend to be spherical with small  $\delta$  value, while natural mineral dust has a larger  $\delta$  value for its irregular shape 5 (Kobayashi et al., 2014). Real-time measurement of  $\delta$  value on a single-particle-based help to avoid the misclassification of aerosol types. Sugimoto et al. (2015) found that backscattering  $\delta$  value in polluted dust was smaller compared to pure Asia dust for the measurement at Seoul. Previous study (Pan et al., 2017) in Beijing indicated that coating processes such as heterogeneous reaction and hygroscopic growth on the surface of dust particles play a vital role in decreasing of depolarization 10 ratio ( $\delta$ ) of particles in coarse mode. As far as we known, long-term measurements of interaction of both anthropogenic pollution and mineral dust and their effect on dust morphological changes in North China are still lacking.

In this study, a comprehensive ground-based measurement of depolarization properties of aerosol particles was performed at an urban site in Beijing, at the State Key Laboratory of Atmospheric Boundary Layer Physics and Atmospheric Chemistry (LAPC, Longitude: 116.37E; Latitude: 39.97N), Institute of Atmospheric Physics/Chinese Academy of Sciences. Morphological variability of ambient aerosol particles were investigated from November 2015 to July 2016 using a 15 Polarization Optical Particle Counter (POPC), and the seasonal characteristics of depolarization ratio ( $\delta$ ) of atmospheric aerosols were explained. Three pollution events including anthropogenic pollution case, typical dust-dominant case and mixed type pollution period were classified according to its size distribution and  $\delta$  value, as well as trajectory analysis, to investigate the interactions between dust particles and pollutants. The objective of this study focuses on the variation of the  $\delta$  value of 20 aerosol particles and its relationship with secondary pollutants. This study represents the first time such long-term observation of ambient aerosol morphology performed in the megacity of Beijing, and provides more applicable data for evaluating the mixing processes of atmospheric aerosols and their climate impact.

## 2 Observation

### 2.1 Instrument overview

The observation of the depolarization properties of single particles in Beijing was performed using a Polarization Optical 25 Particle Counter (POPC) (Kobayashi et al., 2014). The instrument was installed on the second floor of an air-conditioned two-story building. The inlet was ~50 cm above the roof of the building, and ambient air was drawn into room through ½ inch stainless tube with rainproof cap. The total flow rate of inlet sampling air was set to 13 lpm (litres per minute) with a supporting pump. For POPC, the detecting size range was 0.5-10  $\mu\text{m}$ . A polarized laser beam at a wavelength of 780 nm illuminated the particles. The POPC uses a forward scattering light at a scattering angle of 60° to determine the size of particles; backward 30 scattering intensity at 120° is divided into two components with polarizer: p-polarized light is in the plane of the incident and reflected beams, known as the horizontal polarized light, while s-polarized light is perpendicular to the plane. Normally, the ratio of the s-polarized signal to that of the total backward light scattering signal is defined as the depolarization ratio ( $\delta$ ),

which can provide morphological information about the particle (Muñoz and Hovenier, 2011). The acceptance angle (angle of the backscattered light received by the polarizer) for the polarization detector is 45°. To avoid coincidence error (several particles passing through the laser beam simultaneously), sampling flow of the POPC is set to 80 ccm (cubic centimetre per minute) with a dilution flow of 920 ccm.

5 During the observation, POPC was calibrated using standard known-size particles (JSR Life Sciences Corp.) at  $D_p = 0.048 \mu\text{m}$  (SC-0050-D),  $1.005 \mu\text{m}$  (SC-103-S) and DYNOSHERE polystyrene standard aerosols at  $3.210 \mu\text{m}$  (SS-032-P),  $5.125 \mu\text{m}$  (SS-052-P),  $7.008 \mu\text{m}$  (SS-074-P) and  $10.14 \mu\text{m}$  (SS-104-P). Aerosols were generated by a nebulizer at a flow rate of 3.5 L/min, desiccated by passing through a vertically placed 45 cm Perma Casing tube (MD-110-24P, GL Sciences), as the laboratory calibration process Figure S1 showed.  $\delta$  value of typical spherical particles at  $D_p = 5.125 \mu\text{m}$ ,  $7.008 \mu\text{m}$  and  $10.14 \mu\text{m}$  were found to be 0.075, 0.085 and 0.102, and the  $\delta$  value was almost zero for the fine mode particles ( $D_p = 0.048 \mu\text{m}$ ,  $1.005 \mu\text{m}$ ) (Figure S2). The uncertainties of the  $\delta$  value was affected by various factors, including voltage variance of power supply ( $\sigma_{vol}^2$ ), environment water content ( $\sigma_{WC}^2$ ) and complex refraction index ( $\sigma_{nf}^2$ ) of the aerosols, we estimate the uncertainty of  $\delta$  value was < 13%. For comparison, mass concentrations of pollutants in Beijing was obtained from a ground-based state control site (Longitude: 116.40E; Latitude: 39.98N; 2.7 km northeast of LAPC) and corresponding meteorology 10 data from the climatological station (Longitude: 116.48E; Latitude: 39.95N; 9.5 km southeast of LAPC), we analysed the artificial pollution process and special mineral dust cases that occurred in Beijing.

15

Vertical profile of extinction coefficient, depolarization ratio of aerosol particles was concurrently measured using a NIES Lidar system from National Institute for Environmental Studies (<http://www-lidarnies.go.jp/AD-Net>) (Singh et al., 2008; Shimizu et al., 2016). The polarization Mie-Lidar is a powerful instrument for identify the change of optical properties 20 of mineral dust (Shimizu et al., 2004). The data from the Lidar was processed in 15 min resolution to derive the volume depolarization ratio at 532 nm, attenuated backscattering coefficient at 1064 nm and 532 nm and the extinction coefficient estimated for spherical aerosols (mainly air pollutant) and non-spherical particles (mainly natural dust). The energy is 20 mJ /pulse and 30 mJ/pulse for 1064 nm and 532nm laser, and the light is emitted vertically with a pulse repetition of 10 Hz (Shimizu et al., 2016). Telescopes with a diameter of 20 cm (Lidar in Beijing) are used to collect the scattered light from the 25 sky at an observation wavelength of 532 nm.

## 2.2 Dispersion and trajectory analysis

Long-range and mesoscale dispersion of air parcels over the Asia region was simulated using the FLEXPART (FLEXible PARTicle Dispersion Model) Dispersion Model. FLEXPART is a Lagrangian transport and dispersion model (<https://www.flexpart.eu>) developed by Norwegian Institute for Air Research. This model is suitable for the simulation of a 30 large range of atmospheric transport processes (Stohl et al., 2005), which can do with forward simulating to trace particles from source areas and backward simulating to track particles from given receptors. The meteorological fields for FLEXPART are taken from NCEP's (National Centers for Environmental Prediction) reanalysis GDAS (Global Data Assimilation System)

dataset on a  $1^{\circ}$  lat  $\times$   $1^{\circ}$  lon grid, which provides global observation meteorological data at 0000, 0600, 1200 and 1800 UTC and forecast data at 0300, 0900, 1500, and 2100 UTC (<http://nomads.ncep.noaa.gov/pub/data/nccf/com/gfs/prod/>). During the simulation, 1 unit mass of particles considered as an air sample was released from the observation site at 150 m above ground level. The spatial distribution of the footprint region of the air samples was calculated on the 5 days of backward simulation 5 considering flow meteorology, turbulent motions, the sub-grid terrain effect and Earth's water cycle. Besides, a footprint region of air parcels of interest were simulated used the HYSPLIT (Hybrid Single Particle Lagrangian Integrated Trajectory Model) Trajectory Model developed by NCEP (National Centers for Environmental Prediction) and NCAR (National Center for Atmospheric Research), which is based on the Lagrangian transport model ([https://ready.arl.noaa.gov/HYSPLIT\\_traj.php](https://ready.arl.noaa.gov/HYSPLIT_traj.php)) (Stein et al., 2015). The dataset provided for HYSPLIT is the global reanalysis data in GDAS format that was stored for 5 10 weeks per month (<ftp://arlftp.arlhq.noaa.gov/pub/archives/gdas1>). It produces meteorological data four times a day, namely, at 0000, 0600, 1200, 1800 UTC, and the horizontal resolution is  $2.5^{\circ}$  lat  $\times$   $2.5^{\circ}$  lon. The vertical direction is 17 floors, ranging from the ground surface to 10 hPa. Elements, including wind, temperature, humidity, potential height and ground precipitation, are provided. During the simulation, the trajectory ensemble option starts multiple trajectories from the first selected starting 15 location. Each member of the trajectory ensemble is calculated by offsetting the meteorological data by a fixed grid factor (one grid meteorological grid point in the horizontal and 0.01 sigma units in the vertical). Air samples were released at 150 m above ground level from LAPC, and the simulation time of the backward trajectory is 5 days.

### 3 Results and discussion

#### 3.1 Size distribution of ambient aerosols

Hourly-averaged volume size distribution of aerosol from 29 November 2015 to 29 July 2016 is shown in Figure 2a. The 20 particle size was derived according to the calibration curve between the forward scattering intensity and standard spherical particles (Figure S3). Mass concentrations of particle matters were reconstructed on the basis of number concentration of particles measured by POPC and particles density. The particle density was assumed to increase linearly from  $1.77 \text{ g/cm}^3$  ( $0.5 \mu\text{m}$ ) to  $2.2 \text{ g/cm}^3$  ( $10 \mu\text{m}$ ). To test the accuracy of the POPC detection, the  $\text{PM}_{2.5}$  and  $\text{PM}_{10}$  inverted by POPC were compared with the observed data from the Olympic Sport Centre state control station (Figure S4). The correlation coefficients are 0.91 25 and 0.89 (significance level: 0.001) for  $\text{PM}_{2.5}$  and  $\text{PM}_{10}$ , respectively. The result also compared well with commercial optical particle counter (KC52, RION, as shown in Figure S5) especially in the coarse mode size range observation.

It can be seen in Figure 2a that volume size distribution generally had two size modes during the whole observation periods. The occurrence of fine mode (peak at  $\sim 1 \mu\text{m}$ ) was accompanied with increase of RH. The coarse mode ( $4\text{--}8 \mu\text{m}$ ) mainly occurred in the spring when eastward transport of dust events were significant (Lue et al., 2010). According to the POPC 30 observations, totally five main dust episodes (March 3-5; March 16-22; March 30-31; April 9-10; April 28-May 1) happened at the site during observation period. For the cases on March 3-5 and March 16-18, volume size distribution of ambient particles showed two peaks in both fine and coarse mode (Figure S6), suggesting the interaction of anthropogenic pollutant and dust

particles, and high possibility of existence of internally mixed dust particles (discussed in section 3.5). In winter 2015, POPC observed anthropogenic-dominant pollution cases for five times. All of them was related to high emissions for residential heating purpose and unfavourable air diffusion circumstance (Wang et al., 2015). In summer, the volume concentration of aerosols in all size mode were significantly low because of relative moderate anthropogenic emission, better diffusing 5 boundary layer condition and frequent precipitation. Besides, relative strong turbulence in the Planetary Boundary Layer also increase the dry deposition processes of particles.

### 3.2 Seasonal patterns of $d\delta$ value of ambient aerosols

Figure 2b illustrates the size-resolved  $\delta$  value as a function of time during observation period. The  $\delta$  value of particles increased significantly with the size increases. Episodes influenced by mineral dust could be easily discerned due to the increase in both 10 the volume concentration of coarse mode aerosols and the  $\delta$  value of fine mode aerosols. In general, the  $\delta$  value of particles in urban Beijing had prominent seasonal variability with a summer-low and spring-high pattern due to the different composition, origins of aerosols and atmospheric meteorology at the site. The averaged  $\delta$  values of particles in both fine and coarse mode was highest in March 2016 (0.26) and lowest in July 2016 (0.19). This seasonal variability was much obvious in fine mode 15 particles. Figure 2c shows temporal variations of hourly and monthly averaged  $\delta$  values for the typical particle size at 1  $\mu\text{m}$  and 5  $\mu\text{m}$ , the error bar depicts the monthly averaged deviation. For fine particles at  $D_p = 1 \mu\text{m}$ , their  $\delta$  values in winter and summer were  $0.09 \pm 0.01$  and  $0.07 \pm 0.01$  respectively, however they could increase up to 0.2 as they were subject to dust events in spring. The phenomena of coexistence of fine mineral dust with anthropogenic pollutants has been reported by 20 electro-microscopic studies in literatures (Li and Shao, 2009; Li et al., 2011). The daily averaged  $\delta$  at  $D_p = 5 \mu\text{m}$  varied significantly between  $0.12 \sim 0.4$  with a monthly mean value of  $0.3 \pm 0.05$ . We could discern that their  $\delta$  values for 5  $\mu\text{m}$  particles in winter could decrease dramatically down to 0.15, however they had a much small deviation in spring. It was 25 because water-soluble anthropogenic pollutant in winter and summer was substantial. Although  $dV/d\log D_p$  of coarse mode particles was comparatively low, heterogeneous processes on the surface of particles in the coarse mode at high RH condition was inevitable, which may result in decrease in  $\delta$  value.

### 3.3 $\delta$ value of aerosols from different origins

25 The dependence of the hourly-averaged  $\delta$  value of particles at  $D_p = 1 \mu\text{m}$  and  $D_p = 5 \mu\text{m}$  on the wind speed and directions in different seasons are plotted in Figure 3. It can be seen that, the  $\delta$  values at the both size increased when the observation site was prevailing northwest wind, almost irrelevant to the season. For the particles at  $D_p = 5 \mu\text{m}$ ,  $\delta$  values in all direction in spring were generally higher than those in winter and summer because of impact of mineral dust aerosols, and the  $\delta$  values 30 also generally increased with wind speed (Figure 3b), implying of impact from re-suspended road dust or floating dust at strong wind condition. For particles at  $D_p = 1 \mu\text{m}$ , it was only during northwest wind period that the  $\delta$  values were 40~50% higher than other direction (Figure 3d-f). It demonstrated that the morphology of particles in the fine mode were altered significantly

only during dust event. We noted that particles with low  $\delta$  values in all size mode was observed when the site was prevailing southeast wind in summer, indicating of presence of large fraction of spherical particles, and high ambient water content greatly contributed to deliquescence process of soluble component in the atmosphere (Figure 3c and 3f).

In order to understand the region source of air masses in different pollution types and further explain the seasonal characteristics of  $\delta$  values of atmospheric aerosols, the footprint of the air mass in typical anthropogenic pollution cases and mineral dust dominant cases were analysed. Generally speaking,  $PM_{2.5}/PM_{10}$  ratios have been used for identifying the sources of primary pollutant (Chan et al., 2005; Pérez et al., 2008). Higher ratio was generally ascribed to anthropogenic related secondary particles (sulfate, nitrate etc.), and a lower ratio indicate significant contributions mainly re-suspended or fugitive mineral dust particles due to some mechanical processes (Chan and Yao, 2008; Akyuz and Cabuk, 2009; Xu et al., 2017). Here, the specific pollution incidents were identified based on the size-resolved volume distribution and  $\delta$  values. The criterion of  $PM_{2.5} > 250 \mu g/m^3$  and  $PM_{2.5}/PM_{10} \geq 0.8$ , and  $PM_{10} > 150 \mu g/m^3$  and  $PM_{2.5}/PM_{10} \leq 0.4$  were chosen for heavy anthropogenic pollution-dominant and dust-dominant cases, as shown in Table 1.

The 5 days backward trajectories were calculated from HYSPLIT ensemble calculations, resulting in 27 members for all-possible offsets around the release point. The different directions from which the air mass originated to Beijing are shown in Figure 4. For mineral dust-dominant episodes, the air mass mainly originated from large areas in western Mongolia and Gobi Desert, and the footprint pattern represented comparatively large dust loading in the atmosphere in spring. While for anthropogenic pollution-dominant period, air mass passed through Beijing-Tianjin-Hebei region where anthropogenic emission was significantly strong. To note that, the RH along the trajectories was 13.9 % averagely during dust-dominant dominate cases (mostly in spring-time) and 87.6 % in anthropogenic pollution-dominant cases (mostly in winter-time). It means that origin of aerosol particles and their interaction with water vapor as well as consecutively heterogeneous reactions can lead to pronounced morphological changes of particles.

### 3.4 $\delta$ variability of atmospheric aerosols in clean and substandard days

Figure 5a shows the number of substandard days that daily-averaged  $PM_{2.5}$  exceed  $75 \mu g/m^3$ , the secondary standard of Chinese Ambient Air Quality Standard. Figure 5b shows the mean mass concentrations of  $PM_{2.5}$ ,  $PM_{10}$  and  $PM_{2.5}/PM_{10}$  ratio in substandard days. About 26.7% of substandard days was featured by high atmospheric loading of coarse-mode particles ( $PM_{2.5}/PM_{10} < 0.6$ ) in winter-spring time. There were 18 substandard days on December 2015 with mean values of  $199.6 \mu g/m^3$ ,  $240.1 \mu g/m^3$  for  $PM_{2.5}$  and  $PM_{10}$ . A high  $PM_{2.5}/PM_{10}$  ratio (0.83) suggested that anthropogenic pollutants were dominant. We found that, median  $\delta$  value of the particles at  $Dp = 5 \mu m$  (0.27) during substandard days in winter of 2015 was 12.9% lower than that (0.31) on clean days, as shown in Figure 5c. It indicated that during the substandard days the dust particles were more likely to be modified in shape due to the coexistence of huge amount of pollutants. The second most pollution days occurred in March (15 days) and April (14 days), and the  $PM_{2.5}/PM_{10}$  was 0.67 and 0.65 respectively. The  $\delta$  value of particles at  $Dp = 5 \mu m$  particles were almost the same for substandard and clean days. This demonstrated that almost all of the mineral dust particles were in irregular shape.

The peak of  $\delta$  value of the particles at  $D_p = 1 \mu\text{m}$  particles occurred in April,  $0.15 \pm 0.03$  ( $0.13 \pm 0.02$ ) in substandard (clean) days (Figure 5d). The high 90<sup>th</sup> percentile value indicated the observation site was influenced by several intensive dust events in spring. Anthropogenic pollution was dominant in substandard days in summer that  $\text{PM}_{2.5}$  account for 0.76 and 0.87 in  $\text{PM}_{10}$  in June and July.  $\delta$  value of aerosols at  $D_p = 1 \mu\text{m}$  and  $5 \mu\text{m}$  in summer were  $0.07 \pm 0.01$  and  $0.27 \pm 0.03$ , and there were no apparent different for substandard and clean days. This was because under the humid and high oxidizing environment in summer-time, catalysing process (Nie et al., 2012; Dupart et al., 2012) on the surface of mineral dust aerosols affect the hygroscopicity of dust and affect evolution of particle morphology. Previous studies found that mineral dust coexisting with  $\text{NO}_x$  can promote the conversion of  $\text{SO}_2$  to sulfate (He et al., 2014). Nie et al. (2014) also found that mixed plumes provide abundant reactive species, and dust-induced photocatalytic reactions accelerate oxidisation in  $\text{SO}_2$  and volatile organic compounds (VOCs). This implies that pollution days in North China was great possible to induce internal mixing of dust and pollutant, especially in high humid atmospheric environment, and dust-related heterogeneous processes on the dust surface can aggravate the deterioration of air quality as a feedback.

### 3.5 $\delta$ value of different types of aerosols

Li et al. (2011) showed that surface of mineral dust aerosols provide a suitable space for heterogeneous reactions with gaseous pollutants, leading to the changes in size, shape and chemical components. On the basis of depolarization properties of single particles, the evolution of mixing state of dust particles could be estimated properly. Here, three pollution cases were carefully chosen considering the variation of both the volume size distribution and  $\delta$  value anthropogenic pollution, typical dust-dominant case and mixed type pollution period (coexistence of anthropogenic pollutants and dust particles in the atmosphere that caused severe air pollutions). Note as “case A” on December 22-23, 2015, “case B” on April 9-10, 2016 and “case C” on March 4-6, 2016 respectively. In this study, we simulated 5-day footprint region of air mass based on FLEXPART model. The inert particles were released at 0900 UTC each day in 23 December 2015, 9 April 2016 and 4 March 2016. The releasing point was at LAPC in Beijing at 150 m above ground level. The footprint regions for the three cases are shown in Figure 6a-c. The variation of volume concentration of particles as a function of both  $\delta$  value and particle sizes are depicted in Figure 6d-f. For better comparison, the standard volume concentration was normalized to maximum value = 1 using the formula: normalized value = (truth value – minimum) / (maximum - minimum).

#### 3.5.1 Anthropogenic pollution-dominant period

In case A, daily-averaged  $\text{PM}_{2.5}$  was  $281.3 \mu\text{g}/\text{m}^3$  with a  $\text{PM}_{2.5}/\text{PM}_{10}$  ratio of 0.72. The volume concentration of particles in this period had a peak in the submicron range, with a  $\delta$  value of  $< 0.1$  (Figure 6d), reflecting of predominance of secondary formation pollutants. As shown in Figure 7,  $\delta$  value of particles with  $D_p$  less than  $2 \mu\text{m}$  were normally less than 0.12 and increased gradually to  $\sim 0.27$  ( $D_p > 4 \mu\text{m}$ ), implying of influence from dust aerosol, even in typical anthropogenic pollution-dominant period. Footprint of air mass covered west of North China Plains, which are characterized by heavy industrialization and high emissions. (Zhao et al., 2012). As suggested by many previous studies (Ilten and Selici, 2008; Wang et al., 2013; Zhang

et al., 2016; Chang and Zhan, 2017), unfavourable meteorological conditions played an important role in the occurrence of severe pollution. In case A, the RH was ranging 80% ~ 90% from 0000 LST on December 22 to 1200 LST on December 23 and the diffusion condition was weak (wind speed < 1.5 m/s) (Figure S7). Air mass was mostly stagnant within a high emission region, resulted in substantially formation of secondary pollutants from primary pollutant precursors in the atmosphere (Wang 5 et al., 2014).

### 3.5.2 Dust dominant case

In the typical dust-dominant case occurred on April 9-10, 2016. The main body of dust plume was arrived at the site on April 9 with a daily-averaged  $PM_{10}$  was 273.6  $\mu g/m^3$ , and  $PM_{2.5}/PM_{10}$  ratio of 0.33. Footprint analysis shows that air mass originated 10 from western Mongolia and transport rapidly by a strong wind (~ 5 m/s). The vertical structure of the dust extinction coefficient determined by ground-based Lidar measurement indicated that the dust plume present a layered structure while arrive in the observation site (Figure 8 a-b). The lowest dust layer that in the altitude of < 700 m first arrived at Beijing at 0600 LST on April 9 containing huge amount of coarse mode particles with hourly averaged  $PM_{2.5-10}$  reached 395  $\mu g/m^3$  at noon. This layer 15 was lifted up and become mixed with the dust layer at height 1 km on afternoon April 9. Impact of anthropogenic pollutants on this dust event was weak for less pollutant. POPC analysis shows no feature of internally mixed dust particle. The  $dV/dlogD_p$  has a peak at 5  $\mu m$  with a mean  $\delta$  value of 0.34, consistent with the result in western Japan (Pan et al., 2015). The  $\delta$  values of 20 aerosols in coarse mode were found to be about 3 times larger than calibration result (0.07 - 0.1) for standard spherical aerosols (Figure S2), which suggest the coarse mode particles at the site was great non-spherical. To note that, the  $\delta$  values ( $0.18 \pm 0.02$ ) of particles in fine mode was twice higher than that during anthropogenic pollutant-dominant case, indicating the presence of irregular dust particles.

### 3.5.3 Mixed pollution case

The vertical profile of extinction coefficient and depolarization ratio during March 4-6, 2016 are shown in (Figure 8), and evolution of depolarization properties of dust particles were simultaneously observed by POPC. During the occurrence of the 25 dust event on March 4, daily-averaged  $PM_{10}$  was 376.3  $\mu g/m^3$  and  $PM_{2.5}/PM_{10}$  was 0.19, and the dust plume existed at an altitude up to 3.5 km on March 5. At 1200 UTC March 5, the main body of dust plume descended to an altitude of less than 1.5 km. The  $PM_{2.5}/PM_{10}$  concurrently increased to 49 % because of mixing with higher concentration of pollutant and rapid gravitational settlement of large particles.  $\delta$  value (0.28) for particles at 5  $\mu m$  decreased 17.6% on midnight March 5 compared to 0.34 on March 4 (Figure S8). The 5 day back trajectory implied that the air masses were from a convergence air flow of 30 deviating northwest and south streams, being affected by both mineral dust in Midwest China and emissions of anthropogenic pollution in East China. The  $dV/dlogD_p$  in case C has two peaks in both submicron range (0.9  $\mu m$ ) and coarse mode range (4.5  $\mu m$ ) (Figure 7a) corresponding to  $\delta$  values of < 0.1 and  $0.3 \pm 0.2$  on Figure 6f. To be noted, the averaged  $\delta$  value for particles at  $D_p$  larger than 4  $\mu m$  was about 0.3, that was 11.8% lower compared to case B (Figure 7 b). T-matrix simulations

indicated that the aspect ratios of the dust particles were estimated to be 1.48 ( $\delta = 0.30$ ) (Figure S9), presuming that the dust particles was in spheroid shape.

Figure 9 shows the scatter diagram of the averaged particle depolarization ratio (PRD) at 532 nm versus ratio of backscattering coefficient at 1064 nm/532 nm on the two dust cases and an anthropogenic-dominant cases according to Lidar measurement. For comparison, the results from an observation study of mixed type pollution in Seoul (Sugimoto et al., 2015) was also plotted in the figure. As shown, the daily averaged  $\delta a$  value for dust aerosols in case C was  $0.26 \pm 0.1$  with a backscattering averaged color ratio of  $1.21 \pm 0.39$ . It was  $\sim 36.6\%$  lower than the  $\delta a$  value in case B ( $0.41 \pm 0.14$ ), but the color ratio ( $1.32 \pm 0.14$ ) was relatively consistent with case C. The air pollution aerosols had a color ratio of  $0.32 \pm 0.25$  and  $\delta a$  value  $0.1 \pm 0.02$ . The results of  $\delta a$  value in pure dust and polluted dust plume was similar to the study in Seoul, even though the coarse mode aerosols observed in Seoul had a smaller size range due to gravitational settlement of large particles during longer range transport. One possible reason for the decrease in  $\delta a$  value was that the mineral dust did be involved in internal mixing process through trapping or heterogeneous reactions. However, we cannot eliminate the possibility that the decrease of  $\delta a$  was just caused by the external mixing of huge amount of dust and anthropogenic pollutants. Because Lidar observations only provide an averaged  $\delta a$  value of all the particles in the detecting volume, the external mixing of dust particles with substantial amounts of spherical secondary anthropogenic particles could also result in a lower  $\delta a$  value. Which means the environmental impact of transported Asian dust in polluted areas in East Asia may be underestimated since shadow area of Lidar in properly recognize polluted dust particles.

### 3.6 Implication on heterogeneous processes on dust particles

Coarse mode particles observed in North China was reported to contain large amount of Ca (Yuan et al., 2006; Geng et al., 2014), generally existing in the form of  $\text{CaCO}_3$  (component of calcite), which is the most widely investigated component of mineral dust particles. Previous studies indicate that the interaction between water vapor and  $\text{CaCO}_3$  particles was significant. Hatch et al. (2008) showed that the mass of adsorbed water on  $\text{CaCO}_3$  is equal to  $\sim 8\%$  of the mass of dry  $\text{CaCO}_3$  particles at 78% RH. Studies also found that 1-9 monolayers of adsorbed water are formed on  $\text{CaCO}_3$  particles at 50% - 95% RH (Gustafsson et al., 2005; Ma et al., 2012). Actually, the composition of dust particles was complex, may also contain  $\text{SiO}_2$  (component of quartz, illite, feldspar),  $\text{Al}_2\text{O}_3$  (illite) and  $\text{CaO}$  (feldspar), aluminosilicate (kaolinite) etc. These substances are comparatively insoluble and not sensitive to water vapor in the air (Tang et al., 2016). This means the heterogeneous reactions and trapping process on the dust surface was closely related to the dust sources and residential time in the atmosphere. For example, Wang et al. (2011) found that the ratio of Ca component in mineral dust in Beijing was high when air mass was from Loess Plateau, while chemical components of dust from desert/Gobi areas contained more crustal element oxides such as  $\text{SiO}_2$ ,  $\text{Al}_2\text{O}_3$ ,  $\text{Fe}_2\text{O}_3$  (Ta et al., 2003). Dust with inert component require longer transport or residential times before morphology changing.

Here, we investigate the vital roles that ambient air humidity and air pollution content in the air played in the morphological changes of dust particles in Beijing area. The high  $PM_{2.5}/PM_{10}$  ratio indicate that the components of soluble inorganic salts or reactive gases loading in the atmosphere was greatly possible to be relatively high, and in the case of high humidity. It also indicate a high collision probability between pollutant and dust. Therefore, morphology and corresponding  $\delta$  value of particles should be affected. According to our 8-month observation in Beijing, the  $\delta$  value had a general trend of increasing with particle size but decreasing with the  $PM_{2.5}/PM_{10}$ . The decrease degree was not equal for different particle size: for particles at  $D_p = 5 \mu m$ ,  $\delta$  value was  $\sim 0.3$  while  $PM_{2.5}/PM_{10}$  was less than 0.6 and decreased  $\sim 20\%$  when  $PM_{2.5}/PM_{10}$  increased to 1; for particles at  $D_p = 1 \mu m$ ,  $\delta$  value decreased by 42.9% from 0.14 to 0.08 (Figure S10). In fact, atmospheric humidity played a vital role in the observed  $\delta$  value decrease. Figure 10 shows the relationship between the  $\delta$  value of dust particles ( $D_p = 5 \mu m$ ), vapor content (RH) and  $PM_{2.5}/PM_{10}$  in the air. It can be seen,  $\delta$  value of particles in coarse mode decreased as  $PM_{2.5}/PM_{10}$  ratio increased, especially under high RH conditions. For particles at  $D_p = 5 \mu m$ , their  $\delta$  value was generally 0.28 - 0.35 when the ambient air was dry (RH < 10%), and it decreased by  $\sim 28.6\%$  when the ambient RH increase to  $> 90\%$ .  $\delta$  value of for particles at  $D_p = 3 \mu m$  decreased by  $\sim 36.4\%$  (Figure S11). For small dust particles, the interaction of water vapor and pollutant on the surface was more obvious in the change of morphology and reduction in  $\delta$  value. This negative relationship reflected the spheroidization of the dust particles as a result of hygroscopic properties of mineral dust aerosols. Polluted air generally contains abundant  $HNO_3$  (Liang et al., 2007; Shi et al., 2014; Bytnerowicz et al., 2016). Li and Shao (2009) reported that mineral particles are mainly covered with coating including  $Ca(NO_3)_2$ ,  $Mg(NO_3)_2$ , and  $NaNO_3$  in North China. Deeper interaction between alkaline mineral dust and reactive acidic gases and the trapping process of atmospheric secondary inorganic salt modified the hydrophilic state of dust aerosols. According to Sullivan et al. (2009), pure  $CaCO_3$  with diameter of  $\sim 2 \mu m$  need a supersaturation values of 0.6 to 0.9 to be activated, while the soluble salts of  $Ca(NO_3)_2$  and  $CaCl_2$ , are more likely to be activated with supersaturation values ranging from 0.07 to 0.4. This means that the more dust particles become involved in chemical mixing or coagulation process, the more easily they become hydrophilic and are incorporated into cloud processes and effect regional/global climate (Shi et al., 2008; Koehler et al., 2009). Besides, the theoretical simulation of Ishimoto et al. (2010) indicated that a change in refractive index could also affect the  $\delta$  value, the simulation results depicted that the  $\delta$  value showed a levelling off tendency at  $0.31 \pm 0.02$  for the coarse modal particles (Figure S12), which means variations in the particle's refractive index can only explain limited depolarization variability (6%). At present, observation studies for single particle  $\delta$  value combined with aerosol chemical composition analysis are still scant. To clarify the chemical process happened during mix pollution, more observational and experimental results in lab are needed.

## 30 4 Conclusions

Interactions between mineral dust and anthropogenic pollutants has great impact on physical properties and climate effect of dust particles in East Asia. In this study, a long-term observation of atmospheric aerosols in the megacity of Beijing from 29 November 2015 to 29 July 2016 was performed using an Optical Particle Counter equipped with a Polarization detection module (POPC). Combined with trajectory and dispersion model analysis, the temporal variability of depolarization

characterization of aerosols, mixing state of dust particles, and their effect on local air quality were investigated. The major conclusions are as follows: (1) The depolarization ratio ( $\delta$ ) of particles in urban Beijing has significant seasonal variabilities due to different components and origins of aerosols. The averaged  $\delta$  value of particles in both fine and coarse mode was highest in March 2016 (0.26) and lowest in July 2016 (0.19). The seasonal variation of the  $\delta$  value in fine mode particles ( $< 2 \mu\text{m}$ ) showed a more pronounced winter-spring high and summer low pattern owing to emissions as well as weather conditions in different seasons. During the substandard days in Beijing, the decrease of  $\delta$  value of particles in coarse mode implied of internal mixing of mineral dust and pollutant, especially under humid atmospheric conditions. (2) Although both Lidar and POPC could identify impact of dust aerosols, single-particle based depolarization measurement could provide more accurate information about the sphericity of particles, which could indicate the possible modification of morphology of particles as a result of mixing processes. Case studies on the evolution of a typical Asian dust event, we found that the  $\delta$  of dust particles obtained by POPC could decrease by 17.6% with mixing effect of polluted. Volume  $\delta$  value measured by Lidar also showed an obvious decreasing trend, however the interference of substantial amount of small spherical anthropogenic pollutant make it difficult to evaluate their interactions. During a typical polluted dust event, the shape of mineral dust can be modified as a result of heterogeneous processes. In this study,  $\delta$  value of particles at  $D_p = 5 \mu\text{m}$  decreased by 28.6% when RH increase up to 90%. (3) These findings bring attention to comprehensive study on the complex mixing processes and possible mechanisms of morphological change of Asian dust. In addition to Lidar and satellites, single-particle based depolarization measurement could provide a reliable detection method for separating aerosol types and investigating mixing processes of aerosol along the transport. This study also indicate an urgent need for a realistic optical model for predicting the physical changed of Asian dust particles during transport.

## 20 Acknowledgement

This work was supported by the National Natural Science Foundation of China (Grant No. 41675128 and 41620104008). Air quality data was provided by ministry of environmental protection, and meteorological data was from the Chinese meteorological department. The author also thank the NCEP for provision of GDAS dataset, NILU for develop FLEXPART Transport and Dispersion model, and NCAR for exploiting HYSPLIT Trajectory Model collaborating with NCEP.

## 25 References

- Akimoto, H.: Global air quality and pollution, *Science*, 302, 1716-1719, 10.1126/science.1092666, 2003.
- Akimoto, H., Ohara, T., Kurokawa, J.-i., and Horii, N.: Verification of energy consumption in China during 1996–2003 by using satellite observational data, *Atmospheric Environment*, 40, 7663-7667, 10.1016/j.atmosenv.2006.07.052, 2006.
- Akyuz, M., and Cabuk, H.: Meteorological variations of PM<sub>2.5</sub>/PM<sub>10</sub> concentrations and particle-associated polycyclic aromatic hydrocarbons in the atmospheric environment of Zonguldak, Turkey, *J Hazard Mater*, 170, 13-21, 10.1016/j.jhazmat.2009.05.029, 2009.

Cesana, G., Chepfer, H., Winker, D., Getzewich, B., Cai, X., Jourdan, O., Mioche, G., Okamoto, H., Hagihara, Y., Noel, V., and Reverdy, M.: Using in situ airborne measurements to evaluate three cloud phase products derived from CALIPSO, *Journal of Geophysical Research: Atmospheres*, 121, 5788-5808, 10.1002/2015jd024334, 2016.

5 Chan, C. K., and Yao, X.: Air pollution in mega cities in China, *Atmospheric Environment*, 42, 1-42, 10.1016/j.atmosenv.2007.09.003, 2008.

Chan, C. Y., Xu, X. D., Li, Y. S., Wong, K. H., Ding, G. A., Chan, L. Y., and Cheng, X. H.: Characteristics of vertical profiles and sources of PM<sub>2.5</sub>, PM<sub>10</sub> and carbonaceous species in Beijing, *Atmospheric Environment*, 39, 5113-5124, 10.1016/j.atmosenv.2005.05.009, 2005.

10 Chang, W., and Zhan, J.: The association of weather patterns with haze episodes: Recognition by PM<sub>2.5</sub> oriented circulation classification applied in Xiamen, Southeastern China, *Atmospheric Research*, 197, 425-436, 10.1016/j.atmosres.2017.07.024, 2017.

Dupart, Y., King, S. M., Nekat, B., Nowak, A., Wiedensohler, A., Herrmann, H., David, G., Thomas, B., Miffre, A., Rairoux, P., D'Anna, B., and George, C.: Mineral dust photochemistry induces nucleation events in the presence of SO<sub>2</sub>, *Proc. Natl. Acad. Sci. U. S. A.*, 109, 20842-20847, 10.1073/pnas.1212297109, 2012.

15 Geng, H., Hwang, H., Liu, X., Dong, S., and Ro, C. U.: Investigation of aged aerosols in size-resolved Asian dust storm particles transported from Beijing, China, to Incheon, Korea, using low- $\text{Z}^{\text{lt}}/\text{Z}^{\text{gt}}$  particle EPMA, *Atmos Chem Phys*, 14, 3307-3323, 10.5194/acp-14-3307-2014, 2014.

Gustafsson, R. J., Orlov, A., Badger, C. L., Griffiths, P. T., Cox, R. A., and Lambert, R. M.: A comprehensive evaluation of water uptake on atmospherically relevant mineral surfaces: DRIFT spectroscopy, thermogravimetric analysis and aerosol 20 growth measurements, *Atmos Chem Phys*, 5, 3415-3421, 10.5194/acp-5-3415-2005, 2005.

Hatch, C. D., Gierlus, K. M., Shuttlefield, J. D., and Grassian, V. H.: Water adsorption and cloud condensation nuclei activity of calcite and calcite coated with model humic and fulvic acids, *Atmospheric Environment*, 42, 5672-5684, 10.1016/j.atmosenv.2008.03.005, 2008.

25 He, H., Wang, Y., Ma, Q., Ma, J., Chu, B., Ji, D., Tang, G., Liu, C., Zhang, H., and Hao, J.: Mineral dust and NO<sub>x</sub> promote the conversion of SO<sub>2</sub> to sulfate in heavy pollution days, *Sci Rep*, 4, 4172, 10.1038/srep04172, 2014.

Ilten, N., and Selici, A. T.: Investigating the impacts of some meteorological parameters on air pollution in Balikesir, Turkey, *Environ Monit Assess*, 140, 267-277, 10.1007/s10661-007-9865-1, 2008.

30 Jickells, T. D., An, Z. S., Andersen, K. K., Baker, A. R., Bergametti, G., Brooks, N., Cao, J. J., Boyd, P. W., Duce, R. A., Hunter, K. A., Kawahata, H., Kubilay, N., laRoche, J., Liss, P. S., Mahowald, N., Prospero, J. M., Ridgwell, A. J., Tegen, I., and Torres, R.: Global iron connections between desert dust, ocean biogeochemistry, and climate, *Science*, 308, 67-71, 10.1126/science.1105959, 2005.

Kobayashi, H., Hayashi, M., Shiraishi, K., Nakura, Y., Enomoto, T., Miura, K., Takahashi, H., Igarashi, Y., Naoe, H., Kaneyasu, N., Nishizawa, T., and Sugimoto, N.: Development of a polarization optical particle counter capable of aerosol type classification, *Atmospheric Environment*, 97, 486-492, 10.1016/j.atmosenv.2014.05.006, 2014.

35 Koehler, K. A., Kreidenweis, S. M., DeMott, P. J., Petters, M. D., Prenni, A. J., and Carrico, C. M.: Hygroscopicity and cloud droplet activation of mineral dust aerosol, *Geophysical Research Letters*, 36, 10.1029/2009gl037348, 2009.

Kurokawa, J., Ohara, T., Morikawa, T., Hanayama, S., Janssens-Maenhout, G., Fukui, T., Kawashima, K., and Akimoto, H.: Emissions of air pollutants and greenhouse gases over Asian regions during 2000–2008: Regional Emission inventory in ASia (REAS) version 2, *Atmos Chem Phys*, 13, 11019-11058, 10.5194/acp-13-11019-2013, 2013.

40 Li, M., Zhang, Q., Kurokawa, J.-i., Woo, J.-H., He, K., Lu, Z., Ohara, T., Song, Y., Streets, D. G., Carmichael, G. R., Cheng, Y., Hong, C., Huo, H., Jiang, X., Kang, S., Liu, F., Su, H., and Zheng, B.: MIX: a mosaic Asian anthropogenic emission inventory under the international collaboration framework of the MICS-Asia and HTAP, *Atmos Chem Phys*, 17, 935-963, 10.5194/acp-17-935-2017, 2017.

Li, W. J., and Shao, L. Y.: Observation of nitrate coatings on atmospheric mineral dust particles, *Atmos Chem Phys*, 9, 1863-1871, DOI 10.5194/acp-9-1863-2009, 2009.

Li, W. J., Zhang, D. Z., Shao, L. Y., Zhou, S. Z., and Wang, W. X.: Individual particle analysis of aerosols collected under haze and non-haze conditions at a high-elevation mountain site in the North China plain, *Atmos Chem Phys*, 11, 11733-11744, 10.5194/acp-11-11733-2011, 2011.

Lue, Y. L., Liu, L. Y., Hu, X., Wang, L., Guo, L. L., Gao, S. Y., Zhang, X. X., Tang, Y., Qu, Z. Q., Cao, H. W., Jia, Z. J., Xu, H. Y., and Yang, Y. Y.: Characteristics and provenance of dustfall during an unusual floating dust event, *Atmospheric Environment*, 44, 3477-3484, 10.1016/j.atmosenv.2010.06.027, 2010.

Ma, Q., Liu, Y., Liu, C., and He, H.: Heterogeneous reaction of acetic acid on MgO, alpha-Al<sub>2</sub>O<sub>3</sub>, and CaCO<sub>3</sub> and the effect on the hygroscopic behaviour of these particles, *Phys Chem Chem Phys*, 14, 8403-8409, 10.1039/c2cp40510e, 2012.

Muñoz, O., and Hovenier, J. W.: Laboratory measurements of single light scattering by ensembles of randomly oriented small irregular particles in air. A review, *Journal of Quantitative Spectroscopy and Radiative Transfer*, 112, 1646-1657, 10.1016/j.jqsrt.2011.02.005, 2011.

Nie, W., Wang, T., Xue, L. K., Ding, A. J., Wang, X. F., Gao, X. M., Xu, Z., Yu, Y. C., Yuan, C., Zhou, Z. S., Gao, R., Liu, X. H., Wang, Y., Fan, S. J., Poon, S., Zhang, Q. Z., and Wang, W. X.: Asian dust storm observed at a rural mountain site in southern China: chemical evolution and heterogeneous photochemistry, *Atmos Chem Phys*, 12, 11985-11995, 10.5194/acp-12-11985-2012, 2012.

Nie, W., Ding, A., Wang, T., Kerminen, V. M., George, C., Xue, L., Wang, W., Zhang, Q., Petaja, T., Qi, X., Gao, X., Wang, X., Yang, X., Fu, C., and Kulmala, M.: Polluted dust promotes new particle formation and growth, *Sci Rep*, 4, 6634, 10.1038/srep06634, 2014.

Pan, X., Uno, I., Hara, Y., Kuribayashi, M., Kobayashi, H., Sugimoto, N., Yamamoto, S., Shimohara, T., and Wang, Z.: Observation of the simultaneous transport of Asian mineral dust aerosols with anthropogenic pollutants using a POPC during a long-lasting dust event in late spring 2014, *Geophysical Research Letters*, 42, 1593-1598, 10.1002/2014gl062491, 2015.

Pan, X. L., Yan, P., Tang, J., Ma, J. Z., Wang, Z. F., Gbaguidi, A., and Sun, Y. L.: Observational study of influence of aerosol hygroscopic growth on scattering coefficient over rural area near Beijing mega-city, *Atmos Chem Phys*, 9, 7519-7530, DOI 10.5194/acp-9-7519-2009, 2009.

Pérez, N., Pey, J., Querol, X., Alastuey, A., López, J. M., and Viana, M.: Partitioning of major and trace components in PM10-PM2.5-PM1 at an urban site in Southern Europe, *Atmospheric Environment*, 42, 1677-1691, 10.1016/j.atmosenv.2007.11.034, 2008.

Shi, Z., Zhang, D., Hayashi, M., Ogata, H., Ji, H., and Fujii, W.: Influences of sulfate and nitrate on the hygroscopic behaviour of coarse dust particles, *Atmospheric Environment*, 42, 822-827, 10.1016/j.atmosenv.2007.10.037, 2008.

Shimizu, A., Sugimoto, N., Matsui, I., Arao, K., Uno, I., Murayama, T., Kagawa, N., Aoki, K., Uchiyama, A., and Yamazaki, A.: Continuous observations of Asian dust and other aerosols by polarization lidars in China and Japan during ACE-Asia, *Journal of Geophysical Research-Atmospheres*, 109, 10.1029/2002jd003253, 2004.

Shimizu, A., Nishizawa, T., Jin, Y., Kim, S.-W., Wang, Z., Batdorj, D., and Sugimoto, N.: Evolution of a lidar network for tropospheric aerosol detection in East Asia, *Optical Engineering*, 56, 031219, 10.1117/1.oe.56.3.031219, 2016.

Singh, U. N., Sugimoto, N., Asai, K., Matsui, I., Shimizu, A., Jayaraman, A., Nishizawa, T., Hara, Y., Xie, C., Uno, I., Yumimoto, K., Wang, Z., and Yoon, S.-C.: Lidar network observations of tropospheric aerosols, *Proc Spie*, 7153, 71530A, 10.1117/12.806540, 2008.

Stein, A. F., Draxler, R. R., Rolph, G. D., Stunder, B. J. B., Cohen, M. D., and Ngan, F.: NOAA's HYSPLIT Atmospheric Transport and Dispersion Modeling System, *Bulletin of the American Meteorological Society*, 96, 2059-2077, 10.1175/bams-d-14-00110.1, 2015.

Stohl, A., Forster, C., Frank, A., Seibert, P., and Wotawa, G.: Technical note: The Lagrangian particle dispersion model FLEXPART version 6.2, *Atmos Chem Phys*, 5, 2461-2474, DOI 10.5194/acp-5-2461-2005, 2005.

Sugimoto, N., Nishizawa, T., Shimizu, A., Matsui, I., and Kobayashi, H.: Detection of internally mixed Asian dust with air pollution aerosols using a polarization optical particle counter and a polarization-sensitive two-wavelength lidar, *Journal of Quantitative Spectroscopy & Radiative Transfer*, 150, 107-113, 10.1016/j.jqsrt.2014.08.003, 2015.

5 Sullivan, R. C., Moore, M. J. K., Petters, M. D., Kreidenweis, S. M., Roberts, G. C., and Prather, K. A.: Effect of chemical mixing state on the hygroscopicity and cloud nucleation properties of calcium mineral dust particles, *Atmos Chem Phys*, 9, 3303-3316, 10.5194/acp-9-3303-2009, 2009.

Ta, W., Xiao, Z., Qu, J., Yang, G., and Wang, T.: Characteristics of dust particles from the desert/Gobi area of northwestern China during dust-storm periods, *Environmental Geology*, 43, 667-679, 10.1007/s00254-002-0673-1, 2003.

10 Takemura, T., Uno, I., Nakajima, T., Higurashi, A., and Sano, I.: Modeling study of long-range transport of Asian dust and anthropogenic aerosols from East Asia, *Geophysical Research Letters*, 29, 11-11-11-14, 10.1029/2002gl016251, 2002.

Tang, M., Cziczo, D. J., and Grassian, V. H.: Interactions of Water with Mineral Dust Aerosol: Water Adsorption, Hygroscopicity, Cloud Condensation, and Ice Nucleation, *Chem Rev*, 116, 4205-4259, 10.1021/acs.chemrev.5b00529, 2016.

15 Uno, I., Eguchi, K., Yumimoto, K., Takemura, T., Shimizu, A., Uematsu, M., Liu, Z., Wang, Z., Hara, Y., and Sugimoto, N.: Asian dust transported one full circuit around the globe, *Nature Geoscience*, 2, 557-560, 10.1038/ngeo583, 2009.

Venkata, S., and Reagan, J.: Aerosol Retrievals from CALIPSO Lidar Ocean Surface Returns, *Remote Sensing*, 8, 1006, 10.3390/rs8121006, 2016.

20 Wang, L. T., Wei, Z., Yang, J., Zhang, Y., Zhang, F. F., Su, J., Meng, C. C., and Zhang, Q.: The 2013 severe haze over southern Hebei, China: model evaluation, source apportionment, and policy implications, *Atmos Chem Phys*, 14, 3151-3173, 10.5194/acp-14-3151-2014, 2014.

Wang, Q., Zhuang, G., Li, J., Huang, K., Zhang, R., Jiang, Y., Lin, Y., and Fu, J. S.: Mixing of dust with pollution on the transport path of Asian dust--revealed from the aerosol over Yulin, the north edge of Loess Plateau, *Sci Total Environ*, 409, 573-581, 10.1016/j.scitotenv.2010.10.032, 2011.

25 Wang, Q., Sun, Y., Jiang, Q., Du, W., Sun, C., Fu, P., and Wang, Z.: Chemical composition of aerosol particles and light extinction apportionment before and during the heating season in Beijing, China, *Journal of Geophysical Research: Atmospheres*, 120, 12708-12722, 10.1002/2015jd023871, 2015.

Wang, Y., Yao, L., Wang, L., Liu, Z., Ji, D., Tang, G., Zhang, J., Sun, Y., Hu, B., and Xin, J.: Mechanism for the formation of the January 2013 heavy haze pollution episode over central and eastern China, *Science China Earth Sciences*, 57, 14-25, 10.1007/s11430-013-4773-4, 2013.

30 Winker, D. M., Vaughan, M. A., Omar, A., Hu, Y., Powell, K. A., Liu, Z., Hunt, W. H., and Young, S. A.: Overview of the CALIPSO Mission and CALIOP Data Processing Algorithms, *Journal of Atmospheric and Oceanic Technology*, 26, 2310-2323, 10.1175/2009jtecha1281.1, 2009.

Xu, G., Jiao, L., Zhang, B., Zhao, S., Yuan, M., Gu, Y., Liu, J., and Tang, X.: Spatial and Temporal Variability of the PM2.5/PM10 Ratio in Wuhan, Central China, *Aerosol and Air Quality Research*, 17, 741-751, 10.4209/aaqr.2016.09.0406, 2017.

35 Yuan, H., Zhuang, G., Rahn, K. A., Zhang, X., and Li, Y.: Composition and mixing of individual particles in dust and nondust conditions of north China, spring 2002, *Journal of Geophysical Research*, 111, 10.1029/2005jd006478, 2006.

Zhang, Z., Zhang, X., Gong, D., Kim, S. J., Mao, R., and Zhao, X.: Possible influence of atmospheric circulations on winter haze pollution in the Beijing–Tianjin–Hebei region, northern China, *Atmos Chem Phys*, 16, 561-571, 10.5194/acp-16-561-2016, 2016.

5

10

15

20

25

30

**Table****Table 1: Crucial air quality indices for selected pollution cases in Beijing.**

Selected pollution cases	Year/Month/Day	PM <sub>2.5</sub> (μg/m <sup>3</sup> )	PM <sub>10</sub> (μg/m <sup>3</sup> )	PM <sub>2.5</sub> /PM <sub>10</sub>	AQI
Anthropogenic-dominant cases	2015/12/01	490	578	0.85	476
	2015/12/23	255	298	0.86	305
	2015/12/25	477	510	0.94	485
	2015/12/29	279	338	0.83	329
	2016/01/02	266	299	0.89	316
Dust-dominated cases	2016/03/05	58	290	0.20	170
	2016/03/06	73	182	0.40	116
	2016/03/28	70	195	0.36	123
	2016/04/09	54	245	0.22	148
	2016/04/10	41	192	0.21	121
	2016/05/05	62	153	0.40	102
	2016/05/06	57	182	0.31	116

5

10

15

20

25

## Figures

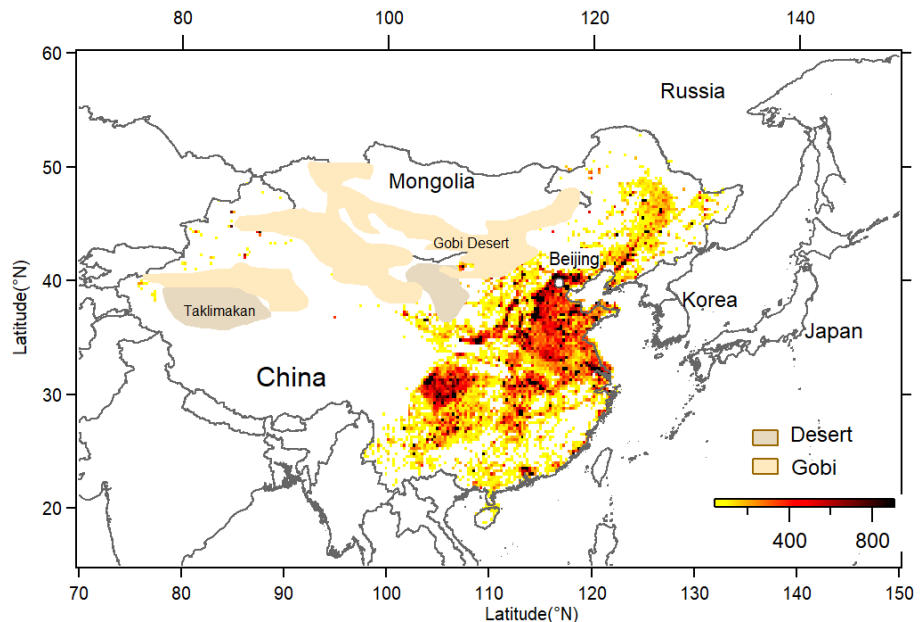


**Figure 1: Geographical location of the observation site in Beijing, PM<sub>2.5</sub> emissions in China and the location of major deserts and the Gobi in East Asia.**

5

10

15

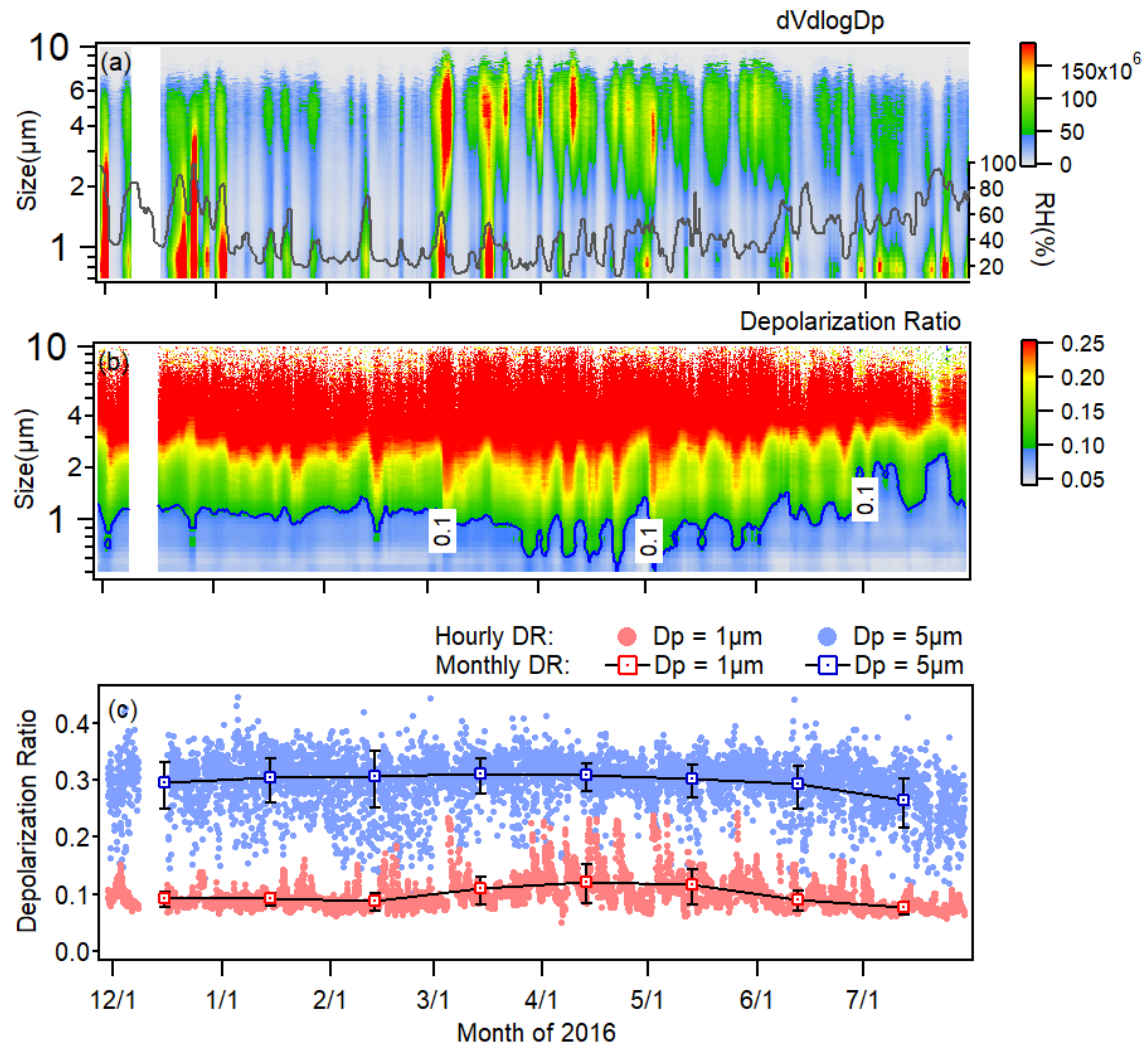
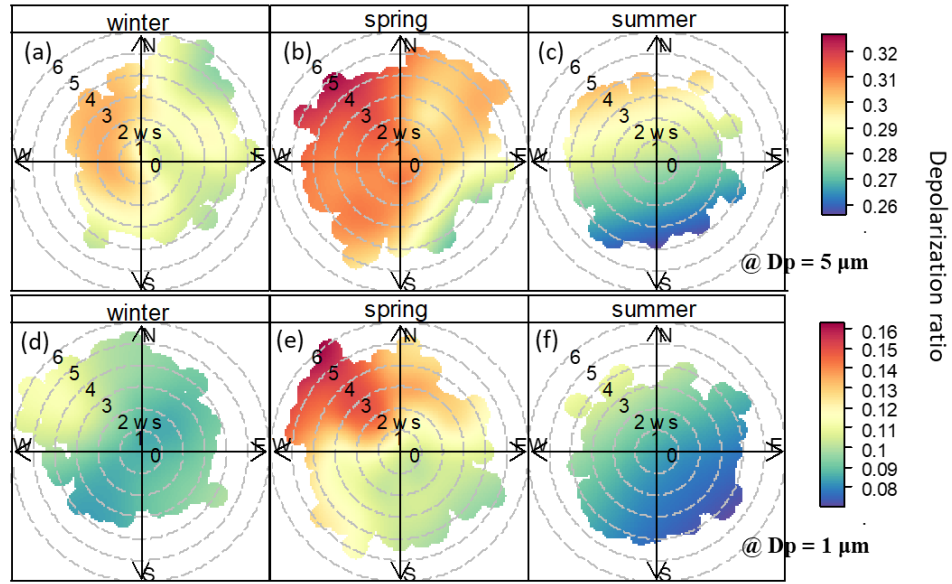


Figure 2: Time series of (a) volume size distributions and RH (gray solid line), (b) size-resolved  $\delta$  value (Green solid line:  $\delta = 0.1$ ), and (c) hourly and monthly averaged  $\delta$  values for fixed-size particles:  $D_p = 1\mu\text{m}$  and  $5\mu\text{m}$  from 29 November 2015 to 29 July 2016. Error bars for monthly averaged  $\delta$  in Figure 2c depict the monthly averaged standard deviation of value.



**Figure 3. Dependence of the hourly-averaged  $\delta$  value of particles at  $D_p = 5 \mu\text{m}$  and  $D_p = 1 \mu\text{m}$  on the wind speed and direction in winter (December, January and February: DJF 2015), spring (March, April and May: MAM) and summer (June and July: JJ) 2016.**

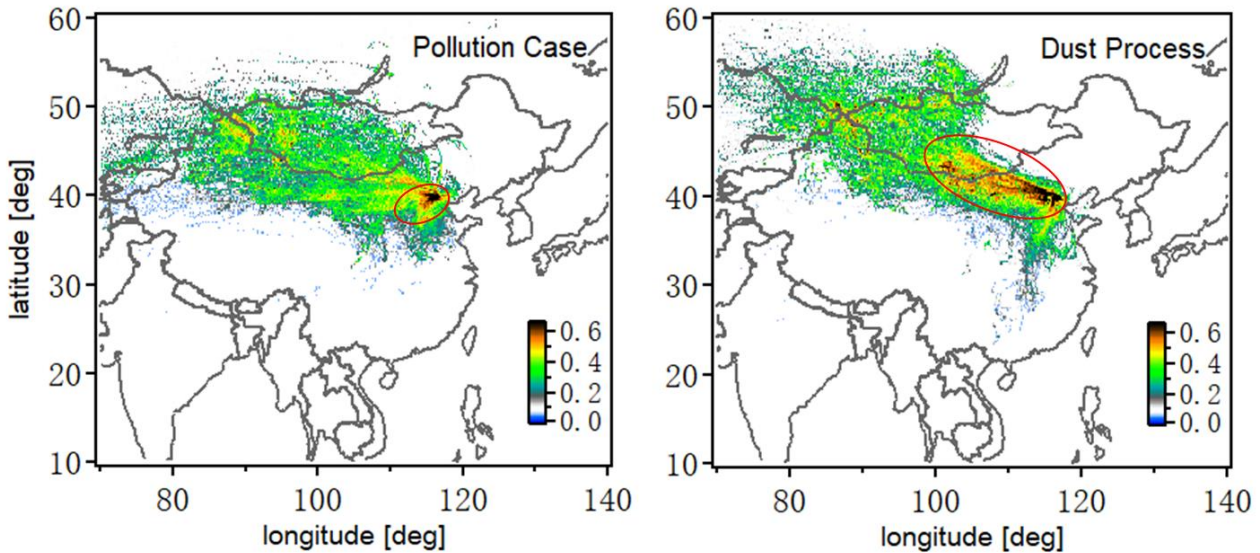
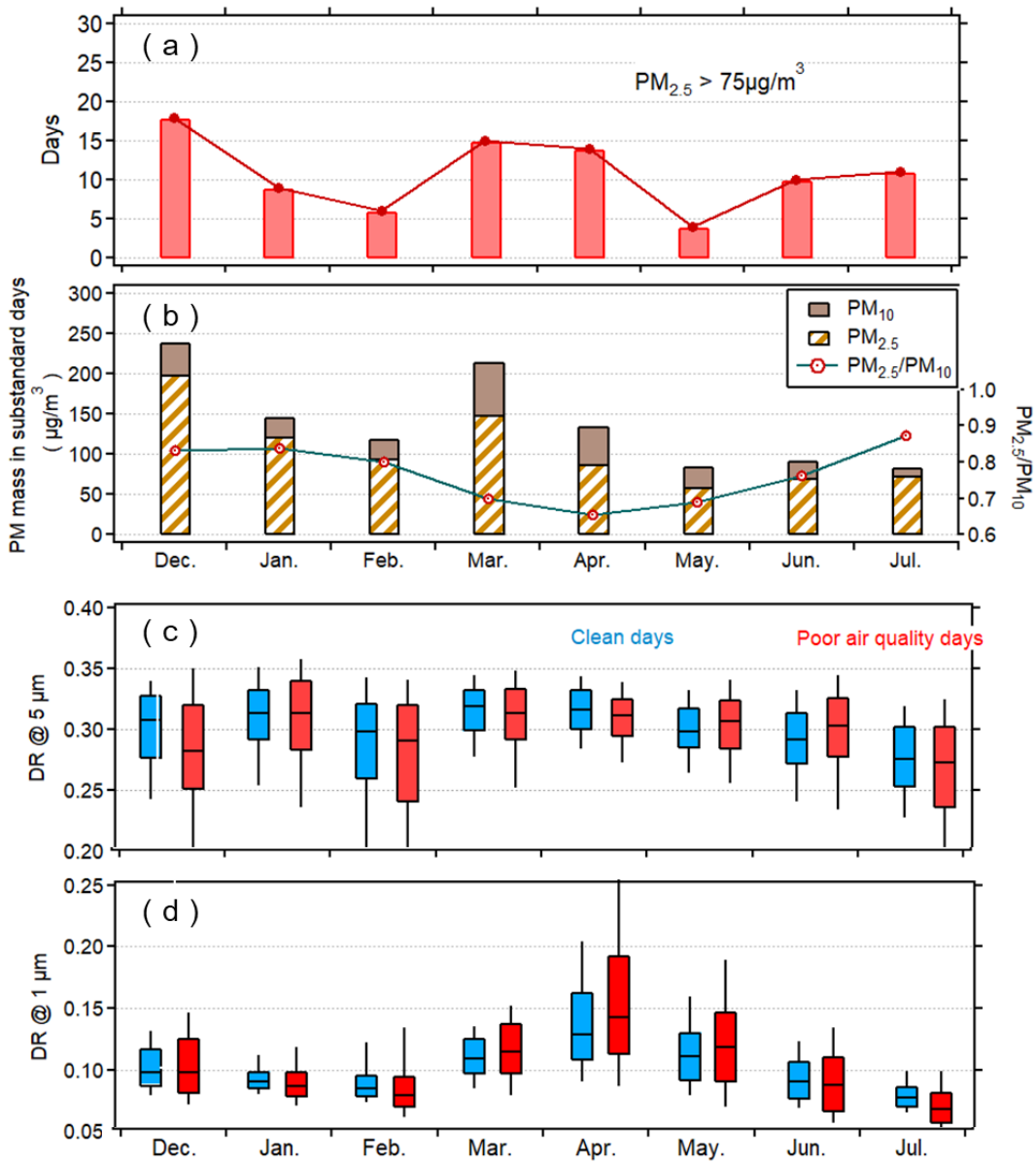
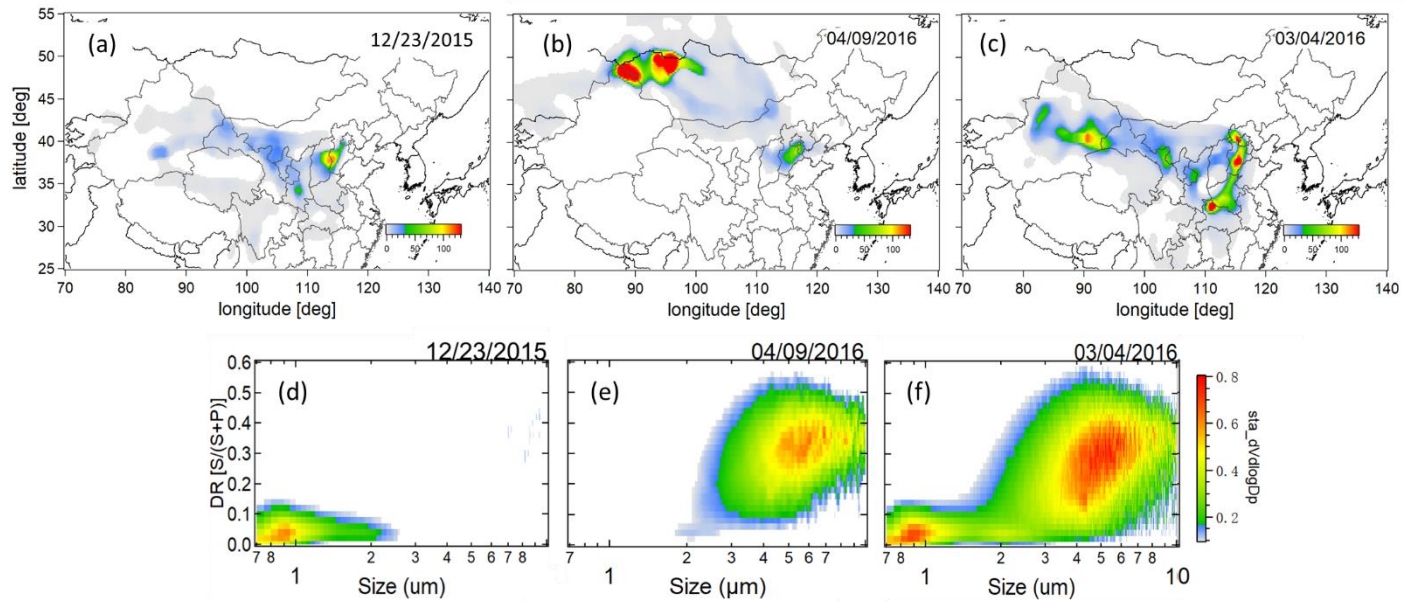


Figure 4: Proportion of different directions from which the air mass over Beijing originated in varying pollution types: severe anthropogenic pollution-dominant case (left), and dust-dominant pollution case (right). The red ellipse represents the major source region of air mass arriving at the site.



5

Figure 5. (a) The number of poor air quality days (daily-averaged  $PM_{2.5}$  exceeding  $75 \mu\text{g}/\text{m}^3$ , the secondary standard of Chinese Ambient Air Quality Standard of  $PM_{2.5}$ , (b) daily averaged mass concentration of  $PM_{2.5}$  and  $PM_{10}$  in the poor air quality days, and ratio of  $PM_{2.5}/PM_{10}$ , box plot of particles  $\delta$  value at (c)  $D_p = 5 \mu\text{m}$  and (d)  $D_p = 1 \mu\text{m}$  in clean days ( $PM_{2.5} < 35 \mu\text{g}/\text{m}^3$ ) and poor air quality days.



**Figure 6. Backward trajectories from Beijing calculated by the FLEXPART dispersion model for (a) the anthropogenic pollution case, (b) the dust-dominant case, and (c) the mixed pollution period. Variation in the standard  $\delta$  value as a function of particle size for corresponding episodes: (d), (e), and (f).**

5

10

15

20

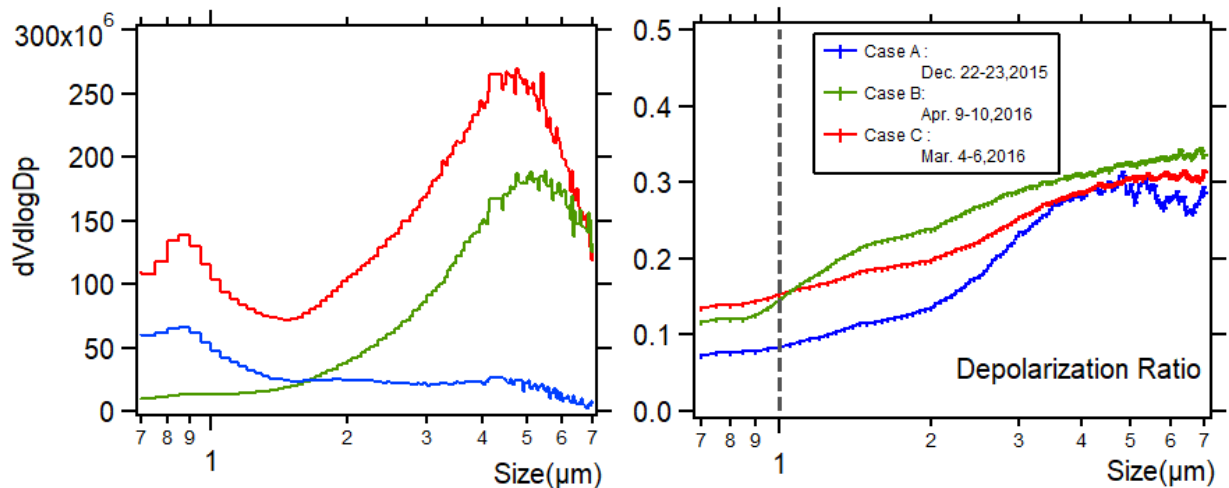
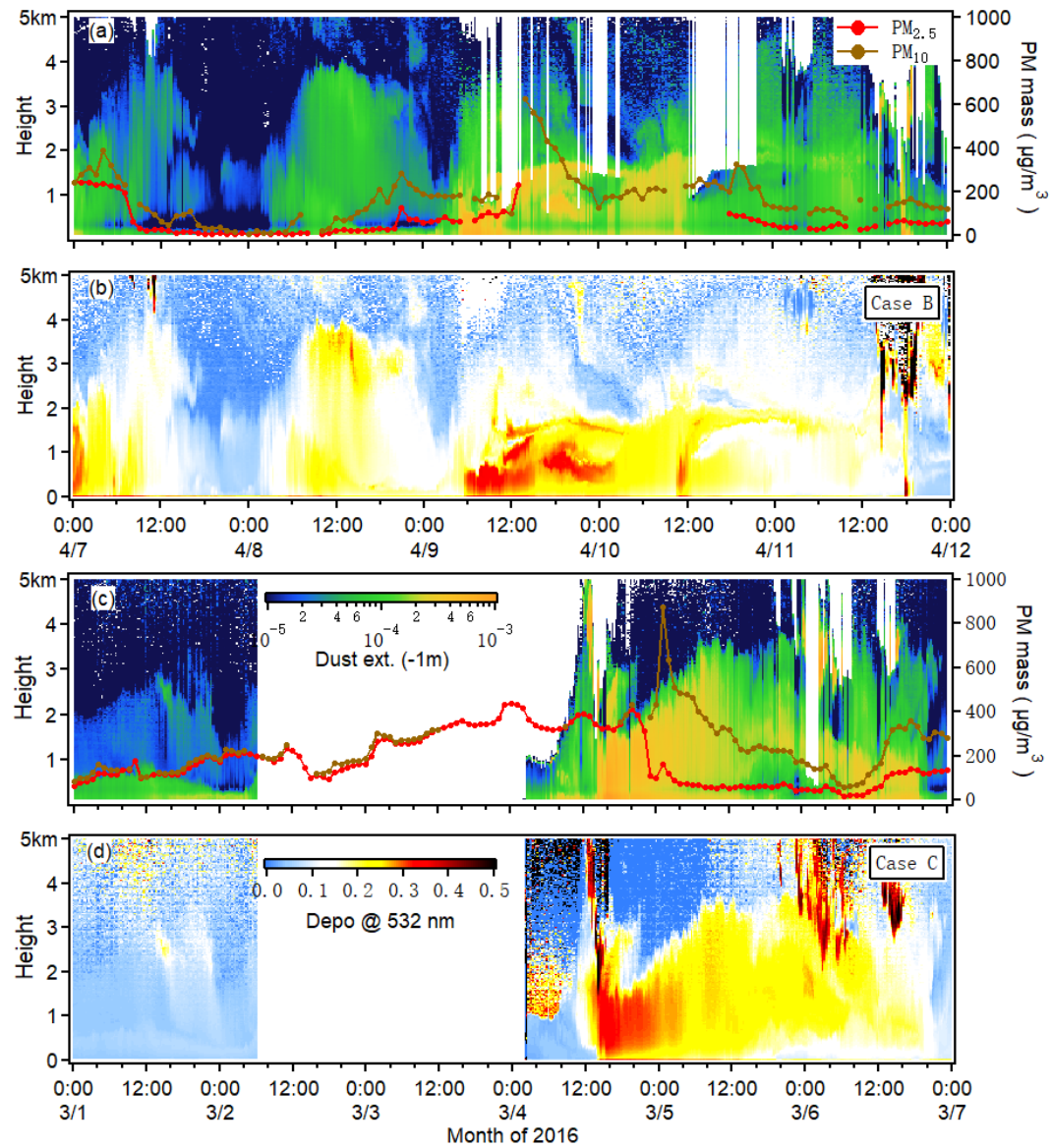


Figure 7. Volume (left) and  $\delta$  value (right) size distribution of aerosols observed in the study cases.



**Figure 8.** Time-height indications of the dust extinction coefficient and the  $\delta$  value at 532 nm derived from polarization-sensitive Lidar measurement in Beijing in case B and case C

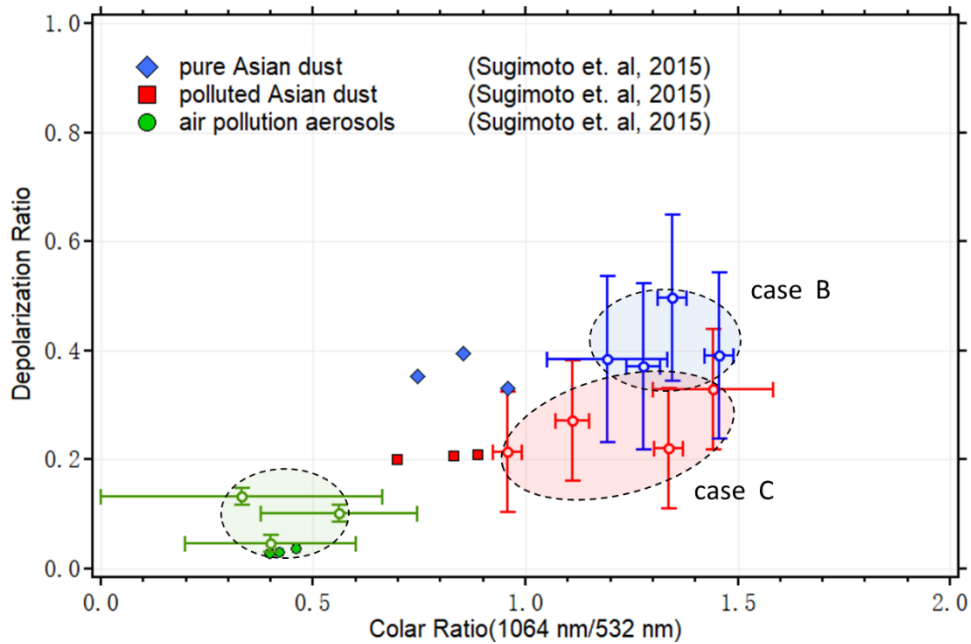


Figure 9. Scatter diagram between the backscattering color ratio (1064 nm / 532 nm) and the particle depolarization ratio at 532 nm for case B (dust-dominant case) and C (polluted dust case) and an anthropogenic-dominant case. The error bars indicate estimates of statistical error. The observations results in Seoul in previous study are displayed in the plot.

5

10

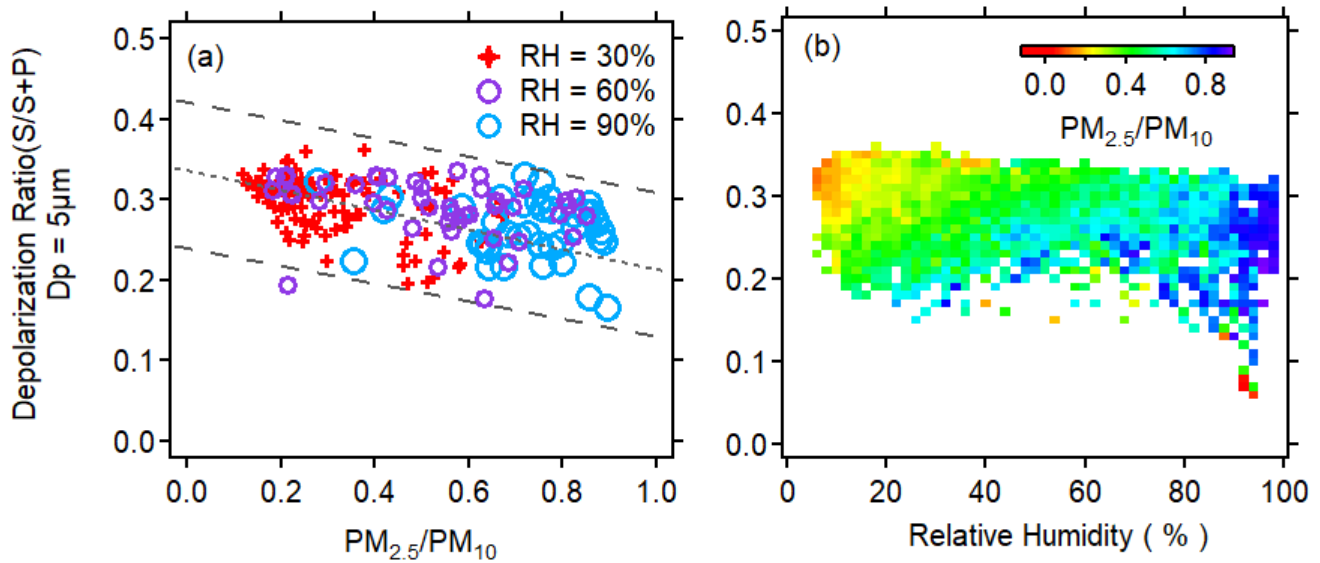


Figure 10. Scatter diagram of the relationship between the  $\delta$  value of dust particles (at  $DP = 5\text{ }\mu\text{m}$ ), vapor content (RH) and  $\text{PM}_{2.5}/\text{PM}_{10}$  in the air.